



Experiment on superadiabatic radiant burner with augmented preheating



H. Wu^a, Y.J. Kim^a, V. Vandadi^b, C. Park^c, M. Kaviany^d, O.C. Kwon^{a,*}

^a School of Mechanical Engineering, Sungkyunkwan University, Suwon, Gyeonggi-do 440-746, Republic of Korea

^b Department of Mechanical Engineering, University of Nevada, Reno, NV 89557, USA

^c Department of Mechanical and Aerospace Engineering, University of Missouri, Columbia, MO 65211, USA

^d Department of Mechanical Engineering, University of Michigan, Ann Arbor, MI 48109, USA

HIGHLIGHTS

- Potential of superadiabatic radiant burners (SRBs) is experimentally confirmed.
- The SRB consists of two-layered porous media, a preheater and radiation rods.
- The SRB can be operated at very fuel-lean condition due to enhanced heat recovery.
- CO/NO_x emissions are reduced compared with the conventional porous radiant burners.
- The SRB is acceptable for practical applications.

ARTICLE INFO

Article history:

Received 21 February 2015

Received in revised form 22 June 2015

Accepted 20 July 2015

Keywords:

Porous burners
Radiant burners
Heat recirculation
Superadiabatic

ABSTRACT

A radiant porous burner with augmented preheating (i.e., superadiabatic radiant burner, SRB) is experimentally investigated. The porous alumina (Al₂O₃) burner with a square cross-section consists of a small-pored upstream section for internally preheating the incoming gas mixture, a large-pored downstream section for establishing flame, a preheater for externally recovering heat from the exiting flue gas and preheating the inlet air for the burner in addition to the internal heat recirculation in the small-pored upstream section, and radiation corridors for extracting heat from the flame and transferring it to radiating disk surfaces. Temperature distribution and combustion stability limits of flame in the SRB and the nitrogen oxide (NO_x) and carbon monoxide (CO) emissions are measured. Results show that the SRB can be operated even at very fuel-lean condition because of the internal and external heat recirculation, showing blow-off and flash-back limits for a given fuel-equivalence ratio. It is observed that the superadiabatic radiation temperature on the disk surfaces is higher than the flue gas temperature at the same axial location, experimentally confirming the previous theoretical and computational results of SRBs. Improved performance of CO and NO_x emissions compared with the conventional porous radiant burners also indicates that the SRB is acceptable for practical application.

© 2015 Elsevier Ltd. All rights reserved.

1. Introduction

In response to the current concerns over climate change and energy security, there has been substantial interest in either developing high-efficiency, low-emission combustion devices or finding alternative energy sources. Porous burners have been considered as one possible technology for achieving the high-efficiency and low-emission since they can recirculate heat from the burned hot

downstream gas to the unburned, incoming cold gas through the porous medium and thus operate under very fuel-lean condition [1,2]. In addition, it is known that the porous burners have the fuel flexibility, implying that alternative and renewable fuels such as low-calorific syngas from waste pyrolysis and landfill gas can be utilized [3].

Recently a novel radiant porous burner with augmented preheating (i.e., superadiabatic radiant burner, SRB) was suggested and computationally investigated [4]. The SRB consists of a small-pored upstream section for internally preheating the incoming gas mixture, a large-pored downstream section for establishing flame, a preheater for externally recovering heat from the exiting

* Corresponding author at: School of Mechanical Engineering, Sungkyunkwan University, 2066 Seobu-ro, Jangan-gu, Suwon, Gyeonggi-do 440-746, Republic of Korea. Tel.: +82 31 290 7465; fax: +82 31 290 5889.

E-mail address: okwon@skku.edu (O.C. Kwon).

flue gas and preheating the inlet air for the burner in addition to the internal heat recirculation in the small-pored upstream section, and radiation corridors for extracting heat from the flame and transferring it to radiating disk surfaces. The two-section porous burners have been studied by various researchers, since the small-pored upstream section can play a role as a flashback arrestor as well as the internal preheater, and the interface between the two sections can stabilize the flame over a wide range of flow rates [5–11]. It was shown that for fuel-lean conditions the external heat recirculation due to the preheater in addition to the internal heat recirculation in the small-pored section can increase the local flame temperature in the SRB beyond the adiabatic flame temperature. Also, extracting and conducting heat from the superadiabatic flame through the embedded radiation corridors (rods), each of which is composed of a finned stem and a radiation disk at the downstream end with high thermal conductivity, the heat is radiated to the target at a higher temperature than the flue gas. Efficiencies of the superadiabatic radiant burner were found to be remarkably enhanced compared with the conventional porous burners.

The concept of external heat recirculation by installing a preheater in a porous burner has not been extensively investigated, though some fundamental studies were reported [12]. Meanwhile, the incorporation of the superadiabatic burners into thermophotovoltaic (TPV) systems in which the direct generation of electricity through thermal radiation is possible can be suggested since the radiation disk surfaces at the downstream end of the radiation corridors are appropriate to effectively radiate heat into photovoltaic cells. Actually the concept of using porous burners instead of conventional cylindrical combustors in the TPV systems has been suggested [13], but the radiation of the heat that is generated from flame into the photovoltaic cells without the radiation corridors is not effective since the flame is submerged in the porous medium. Thus, the SRBs seem to have a significant improvement in the performance compared with the conventional porous burners, particularly for the specific applications such as TPV systems that require effective radiation to the target. Considering that the concept of the SRB has been suggested via a computational investigation, it is needed to experimentally demonstrate it.

In view of the above considerations, in this study we aim to experimentally demonstrate the novel concept of the SRB, with the following specific objectives. The first objective is to design and fabricate a laboratory scale SRB for demonstrating the concept. The second objective is to measure the combustion stability limits of fuel-lean propane (C_3H_8)/air flames in the SRB at normal temperature and pressure (NTP), including the blow-off (i.e., high-stretch extinction) limits and the flashback (i.e., low-stretch) limits, in order to provide the fundamental database of steady-state operating limits of the SRB. The third objective is to confirm the superadiabatic effects of the SRB. We measure the temperature distribution in the porous medium to observe if the peak flame temperature is higher than the adiabatic flame temperature of the corresponding fuel/air mixture. Temperatures of radiating disk surfaces and the flue gas at the same axial location are also measured to observe if the former is higher than the latter. The fourth objective is to measure the nitrogen oxide (NO_x) and carbon monoxide (CO) emissions of the premixed C_3H_8 /air flames in the SRB in order to observe if the SRB can exhibit NO_x and CO reduction. Finally, we estimate the thermal efficiencies of the SRB.

The configuration of the designed SRB, the combustion stability limits and temperature distribution of the premixed C_3H_8 /air flames in the SRB, the superadiabatic effects of the SRB and the CO and NO_x emissions and efficiencies of the SRB will be subsequently presented, following the descriptions of the experimental methods used during this investigation.

2. Experimental methods

The superadiabatic radiant burner with two porous sections (i.e., two-layer porous media), radiation rods embedded in the porous media and a preheater is considered for the present investigation since it is expected to experimentally demonstrate the superadiabatic effects. A diagram of the experimental apparatus used in this study is shown in Fig. 1. It consists of a test SRB, a fuel–air mixture supply system, a ventilation system, thermocouples for measuring temperature distribution in the SRB, a gas analyzer for measuring NO_x and CO emissions and a digital camera (Sony A65) for recording flame and radiation images.

Air (21% oxygen (O_2)/79% nitrogen (N_2) in volume, purity >99.9%) and C_3H_8 (purity >99.9999%) are supplied respectively to a preheater and to a mixing chamber using commercial mass flow controllers (Aera: 0–5 slm and MKS: 0–200 slm) with accuracy $\pm 1.0\%$ of full scale. The mass flow controllers are calibrated using a bubble meter. Air is preheated through the preheater and then it is delivered to the mixing chamber. The preheater is a spiral fin tube with the inner diameter of 10.2 mm (stainless steel, SUS316L) and is located between the downstream end of the porous medium of the SRB and the radiation disks of the radiation rods. Thus, heat in exhaust gas is recovered to preheat fresh air in the preheater. The preheated air and fuel are mixed in the mixing chamber and are issued from the bottom of a distributor ($68 \times 68 \times 60 \text{ mm}^3$) that is filled with stainless steel beads with an average bead diameter of 1.5 mm for obtaining uniform flow. The distributor is windowed to detect flashback using quartz. The preheated air–fuel mixture is fed into the porous medium of the SRB with uniform flow.

The test SRB is two-layered: a porous medium with fine alumina (Al_2O_3) foam (PM1: 60 ppi (pores per inch), $68.0 \times 68.0 \times 40.0 \text{ mm}^3$, Drache Inc.) upstream and the other porous medium with coarse Al_2O_3 foam (PM2: 20 ppi, $68.0 \times 68.0 \times 40.0 \text{ mm}^3$, Drache Inc.) downstream. The sides of porous media are surrounded by the heat-insulated case with thickness of 5.0 mm (SUS316L, $78 \times 78 \times 140 \text{ mm}^3$). The preheated air–fuel mixture is ignited at the exhaust outlet of the burner by a torch-igniter. Once the mixture is ignited, the flame moves backward and is stabilized in the PM2 or on the interface between the PM1 and PM2. Heat from the flame is extracted through the fins around the stem of the embedded radiation rods (silicon carbide, SiC), conducted through the stem and radiated at the radiation disk surface. Figs. 2 and 3 show the photographs of the assembled and disassembled SRB and the typical images of the radiating PM2 and disks, respectively.

R-type thermocouples with a bead diameter of $250 \pm 20 \mu\text{m}$ and an accuracy of $\pm 0.25\%$ are used to measure the temperature (T) distribution in the PM2. A stage on which the thermocouples are fixed can move through a hole that is drilled along the axial centerline, identifying the maximum flame temperature and its location. The preheated air temperature is measured using K-type thermocouples with a bead diameter of $250 \pm 20 \mu\text{m}$ and an accuracy of $\pm 0.75\%$. K-type thermocouples are also used to measure the radiation disk surface temperature and the exhaust gas temperature at the same axial location as the disk surface. The disk surface temperature and the exhaust gas temperature are obtained by averaging measurements at the same axial location but different points.

The combustion stability limits of fuel-lean C_3H_8 /air flames in the SRB are measured by varying the fuel-equivalence ratio ϕ and the burner inlet velocity V that is defined as the total volume flow rate of the mixture divided by the cross-sectional area of the PM1. Propane has been chosen as fuel since it can be used in practical applications. Once a flame is stabilized in the PM2 as aforementioned, ϕ is set to a fixed value and then V is varied to find the combustion stability limits. Given ϕ two combustion stability

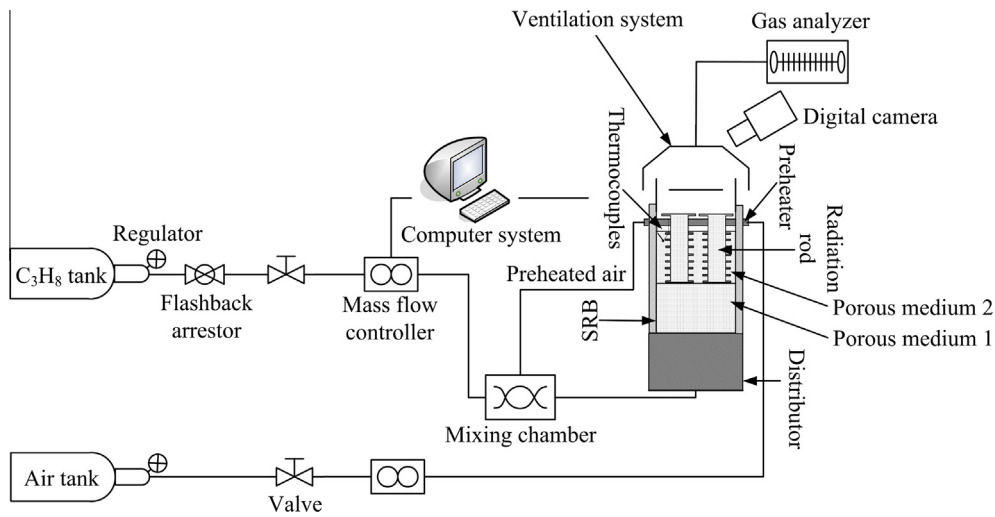


Fig. 1. Schematics of experimental apparatus.

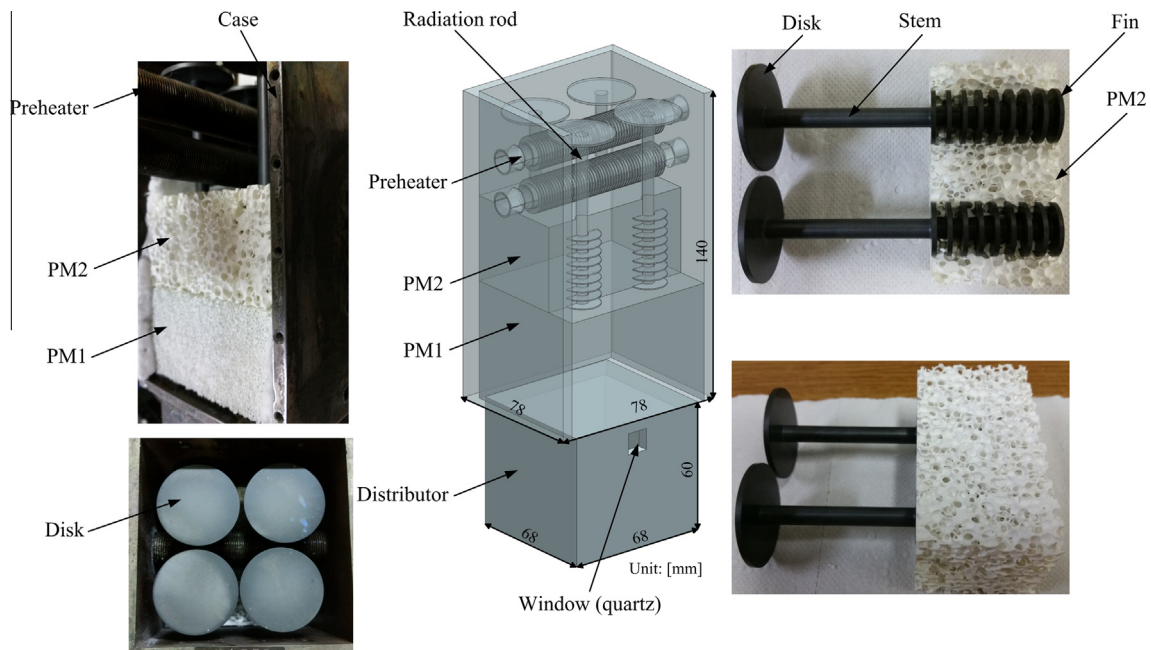


Fig. 2. Photographs of assembled and disassembled SRB.

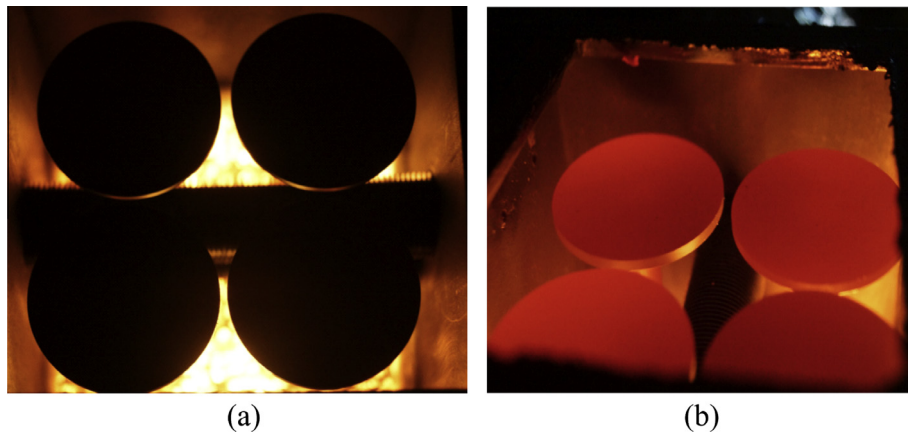


Fig. 3. Images of radiating PM2 (a: warming-up condition) and glowing radiation disks (b: steady condition).

limits are observed in general: the flashback (i.e., low-stretch) limits at low V s and the blow-off (i.e., high-stretch extinction) limits at high V s. For some conditions no blow-off limits were obtained because of the limited capability of the present apparatus. The concentrations of NO_x and CO are also measured in the ventilation tube using a gas analyzer (Testo 350-XL) with an accuracy of 0.1–1.0 ppm: the probe is located on the center of the ventilation path. Final results are obtained by averaging measurements of 4–6 tests at each condition. Experimental uncertainties (95% confidence) for V and T are less than 5%. At NTP (298 ± 3 K) experiments were carried out for $\phi = 0.28$ – 0.65 and $V = 0.092$ – 0.459 m/s.

3. Results and discussion

3.1. Configuration and dimensions of SRB

The final configuration and dimensions of the two-layered SRB with a preheater and radiation rods as briefly described in Section 2 (Fig. 2) have been determined from the earlier computational study of the concept of the SRB [4].

In order to use a simple structured, uniformly radiating burner, a square cylindrical configuration is chosen as the basic geometry of the SRB, and the external heat-recirculation concept of recovering heat from exhaust gas for preheating fresh air with the preheater is adopted. Heat from the flame stabilized in the PM2 is extracted through the fins around the stem of the embedded radiation rods, conducted through the stem and radiated at the radiation disk surface. Considering the limited capability of the present mass flow controllers, the cross-sectional area of the PM 1 and PM 2 has been determined, and four radiation rods are embedded into the PM2. Based on the earlier computational study of the SRB [4] and the feasibility of fabrication, the pore size and length (thickness) of the PM1 and PM2 and the dimensions of the preheater and the stem, fins and disk of the radiation rods have been also determined. The measured preheated air temperature through the preheater for the present tests ranges from 453 to 501 K, i.e., the temperature gain compared with the air supply temperature when the preheater is not installed is 155–203 K, mainly being affected by the fuel-equivalence ratio. Specifications of the major components of the SRB, including the detailed dimensions and materials, are provided in Table 1.

3.2. Combustion stability limits and temperature distribution in SRB

The combustion stability limits of fuel-lean C_3H_8 /air flames in the SRB are measured to provide the fundamental database of steady-state operating limits of the present SRB at NTP. Once a flame is stabilized in the PM2 as described in Section 2, ϕ is set to a fixed value and then V or the firing flux of fuel (\dot{Q}'' , based on lower heating value) is varied to find the combustion stability limits.

Fig. 4 shows the combustion stability limits on a \dot{Q}'' – ϕ diagram for fuel-lean premixed C_3H_8 /air flames in the SRB at NTP. Given ϕ two combustion stability limits are observed in general: the flashback (i.e., low-stretch) limits at low \dot{Q}'' s and the blow-off (i.e., high-stretch extinction) limits at high \dot{Q}'' s. The flashback limits are observed when the local burning velocity exceeds V , while the blow-off limits are observed due to insufficient residence times of the supplied fuel–air mixture. For some conditions no blow-off limits were obtained because of the limited capability of the present apparatus, particularly the air supply system, since very high air flow rates are required for those conditions. Error bars for some data points indicate typical variations for the present measurements. With increasing ϕ , \dot{Q}'' s at both the flashback and blow-off

Table 1
Specifications of major SRB components.

Components	Parameters	Values
PM1	Materials	Alumina (Al_2O_3)
	Width (height)	68.0 mm
	Length	40.0 mm
	Porosity	0.835
	Pore size	60 ppi
	Thermal conductivity	0.2 W/m K
PM2	Materials	Al_2O_3
	Width (height)	68.0 mm
	Length	40.0 mm
	Porosity	0.870
	Pore size	20 ppi
	Thermal conductivity	0.1 W/m K
Radiation rods	Materials	Silicon carbide (SiC)
	Stem diameter	6.0 mm
	Fin diameter	16.0 mm
	Fin thickness	1.5 mm
	Fin pitch	333 m^{-1}
	Disk diameter	32.0 mm
	Disk thickness	2.0 mm
	Length	90.0 mm
Preheater (fin tube)	Materials	Stainless steel (SS316L)
	Inner diameter	10.2 mm
	Fin diameter	16.0 mm
	Fin thickness	1.0 mm
	Fin pitch	666 m^{-1}
	Tube thickness	0.5 mm
	Length	70.0 mm

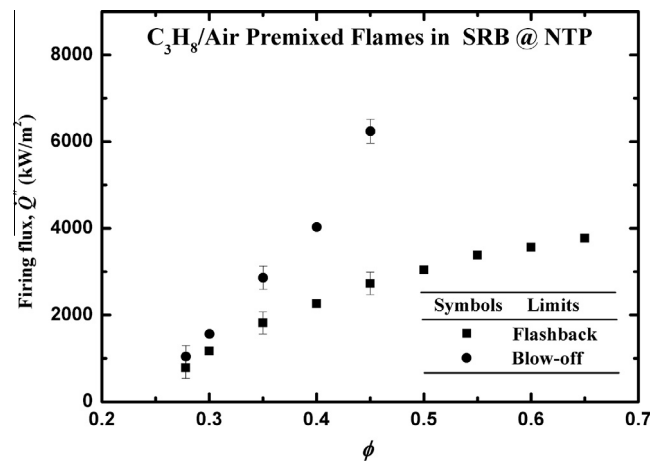


Fig. 4. Combustion stability limits on \dot{Q}'' – ϕ diagram for fuel-lean premixed C_3H_8 /air flames in SRB at NTP.

limits increase. This tendency is observed since under the fuel-lean condition the burning velocities of C_3H_8 /air flames also increase with enhanced ϕ . However, the blow-off limits increase more sharply than the flashback limits, indicating that the former is more sensitive to fuel composition than the latter and thus showing an effect of widening the stable operating range of the SRB for enhanced ϕ . This observation was somewhat expected since similar tendencies are observed for porous radiant burners with no external heat recirculation [14] and tube type gas burners [15]. The ϕ limit where the flashback and blow-off limits are merged is estimated to be around 0.25, which is considered to be substantially extended compared with the limits for conventional porous radiant burners having a configuration and dimensions similar to the present SRB since preheated air is supplied to the burner inlet for the SRB while ambient air at normal temperature for the conventional porous burners.

Fig. 5 shows the combustion stability limits on a $V-\phi$ diagram for fuel-lean premixed C_3H_8 /air flames in the SRB at NTP. Similar to the combustion stability limits on the $\dot{Q}''-\phi$ diagram (Fig. 4), the flashback and blow-off limits are observed for a given ϕ , except for some conditions where the blow-off limits could not be measured due to the limited capability of the present air supply system. Again, error bars for some data points indicate typical variations for the present measurements. With increasing ϕ , V_s at both the flashback and blow-off limits increase, showing a sharper increase for the blow-off limits, similar to the \dot{Q}'' limits in Fig. 4; however, the flashback limits are almost constant beyond $\phi = 0.4$. This tendency is observed since with increasing ϕ the total volume flow rate of the fuel–air mixture does not change remarkably though fuel composition increases.

To understand flame structure in the present SRB at NTP and to provide an additional database at steady-state operating condition the temperature distribution in the PM2 has been measured. Fig. 6 shows the temperature distribution along the axial centerline of the PM2 for premixed C_3H_8 /air flames of $\phi = 0.48$ and various fuel flow rates (1000–1400 sccm). All the flames in the figure are under steady-state operating condition, and each firing condition was determined by controlling it to establish a flame at a proper position for various conditions. Also, those stable operating conditions are confirmed from the combustion stability limits in Figs. 4 and 5. As shown in Fig. 6, all the flames are established quite downstream from the interface between the PM1 and PM2. With increasing fuel flow rates the peak temperature is enhanced, though its location does not seem to be sensitive to the flow rate within the current test range and thus no consistent tendency is observed, showing the locations at the peak temperature between 20 and 25 mm downstream from the interface. The tendency of the enhanced peak temperature with increasing fuel flow rates is observed since the flame is intensified with the increased amount of supplied fuel. The superadiabatic effects of the present SRB shown in Fig. 6 will be discussed in Section 3.3.

In order to observe the effects of ϕ on flame structure in the SRB, the temperature distribution in the PM2 at enhanced ϕ has been measured. Fig. 7 shows the temperature distribution along the axial centerline of the PM2 for premixed C_3H_8 /air flames of $\phi = 0.60$ and various fuel flow rates (1000–1400 sccm). Similar to the flames of $\phi = 0.48$ in Fig. 6, all the flames in the figure are under steady-state operating condition and are established downstream from the interface between the PM1 and PM2. Also, with increasing fuel flow rates temperature is generally enhanced due to the intensified burning. Although no consistent tendency is still observed

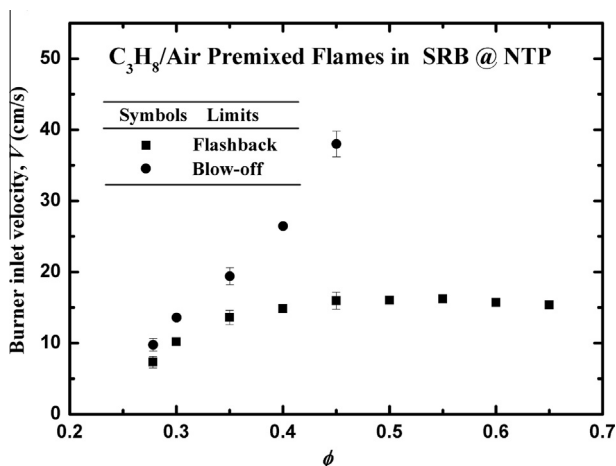


Fig. 5. Combustion stability limits on $V-\phi$ diagram for fuel-lean premixed C_3H_8 /air flames in SRB at NTP.

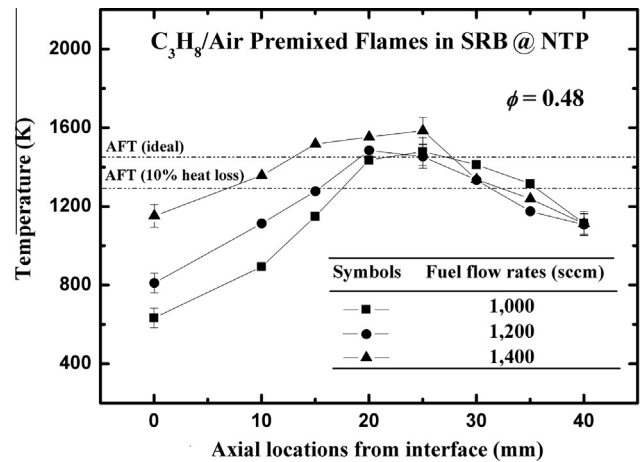


Fig. 6. Temperature distribution along axial centerline of PM2 for premixed C_3H_8 /air flames of $\phi = 0.48$ and various fuel flow rates.

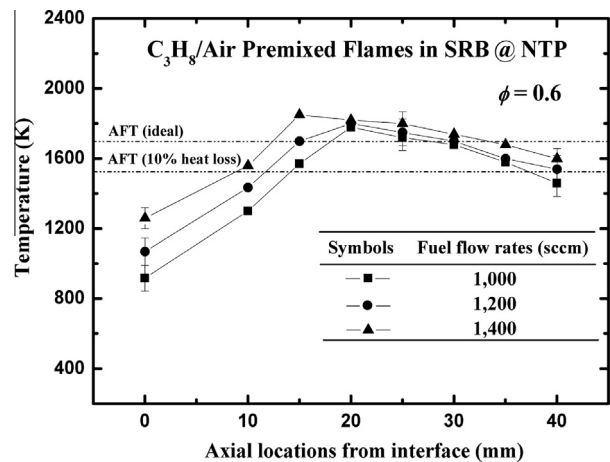


Fig. 7. Temperature distribution along axial centerline of PM2 for premixed C_3H_8 /air flames of $\phi = 0.60$ and various fuel flow rates.

for the location at the peak temperature in terms of fuel flow rates, however, all the flames somewhat shift upstream compared with the flames at fuel-leaner condition in Fig. 6, showing the locations at the peak temperature between 15 and 20 mm downstream from the interface. This is observed since the burning velocities are enhanced with increasing ϕ and thus the fuel–air mixture burns relatively fast for a fixed fuel flow rate. The flame location in the PM2 is expected to be one of the important design parameters for the practical applications of the SRB, e.g., TPV devices. For instance, if the flame is established downstream in the PM2, temperature of the radiation disks can increase and then photovoltaic performance may improve. Also, the effects of preheating air in the preheater of the SRB can be enhanced. However, high exhaust gas temperature cannot be avoided, implying that the overall system efficiency degrades. Thus, further studies regarding the effects of the flame position in the SRB are needed when the overall performance of practical systems is considered. Again, the superadiabatic effects of the present SRB shown in Fig. 7 will be discussed in Section 3.3.

3.3. Superadiabatic effects

The superadiabatic effects of the SRB are examined to experimentally confirm the unique features, comparing the measured

peak flame temperature in the PM2 with the adiabatic flame temperature as well as temperature of radiating disk surfaces with the flue gas at the same axial location.

Figs. 6 and 7 which show the temperature distribution in the PM2 for the fuel-lean premixed C₃H₈/air flames as discussed in Section 3.2 also include the adiabatic flame temperature (AFT) of the corresponding fuel–air mixtures. The adiabatic flame temperature is computed using the NASA CEA (Chemical Equilibrium with Applications) code [16]. As shown in Fig. 6 the peak temperature for all the flames is higher than the AFT, which indicates the superadiabatic effects of the SRB. Considering heat losses to the surroundings even with thermal insulation under practical operating condition, this superadiabatic effect is remarkable. For example, the peak temperature is much higher than the actual AFT that is estimated when 10% heat losses are assumed. The AFT and the AFT with 10% heat losses for the premixed C₃H₈/air flame of $\phi = 0.48$ at NTP are respectively 1456 and 1310 K, indicating the difference between the AFT and the maximum peak temperature of 124 K (i.e., the maximum peak temperature 8.5% higher than the AFT). Fig. 7 for the flames of the enhanced $\phi (= 0.60)$ also shows a similar observation with the AFT of 1700 K, the AFT with 10% heat losses of 1530 K and the difference between the AFT and the maximum peak temperature of 150 K (i.e., the maximum peak temperature 8.8% higher than the AFT). Thus, the superadiabatic effects do not change significantly with ϕ variations, though flames somewhat shift upstream with increasing ϕ . Of course, these superadiabatic effects of the SRB are observed due to the external heat recirculation through the preheater as well as the internal heat recirculation through the PM1.

In addition to the superadiabatic effects in terms of the peak temperature in the PM2, temperature of radiating disk surfaces and the flue gas at the same axial location are also measured to observe if the former is higher than the latter, which is expected from the earlier computational study of the concept of the SRB [4]. Fig. 8 shows the measured disk and flue gas temperature at the same axial location in terms of fuel flow rates for premixed C₃H₈/air flames of $\phi = 0.45$ in the SRB at NTP. Both the disk and flue gas temperatures increase with increasing fuel flow rates because the burning in the PM2 is intensified. Due to the superadiabatic effects of the SRB, i.e., the preheating and the separate heat transfer through the radiation rods having high thermal conductivity, the radiating disk surface temperature is higher than the flue gas temperature for all the tests. The difference between two temperatures is 53–67 K, which seems to be reasonable since the computational study where no heat losses to the surroundings (particularly

through the side walls of the burner case) are assumed shows the difference up to 81 K [4], though the dimensions of the SRB and the test conditions are somewhat different from those in the present study. The disk temperature higher than the flue gas temperature may result in higher radiation efficiency, which will be discussed in Section 3.4. Thus, the results in Figs. 6–8 experimentally and clearly demonstrate the superadiabatic effects of the SRB.

3.4. CO/NO_x emissions and efficiencies

In order to evaluate if the SRB can exhibit CO and NO_x reduction compared with conventional gas burners for its practical application, the CO and NO_x emissions of the premixed flames in the SRB have been measured. Also, the thermal efficiencies of the present SRB are estimated, though it has not been optimally designed considering various parameters.

Fig. 9 shows CO emissions from the exhaust gas as a function of fuel flow rates for premixed C₃H₈/air flames of various fuel-equivalence ratios ($\phi = 0.3–0.6$) in the SRB at NTP. In general, the CO concentration is below 25 ppm, except for very fuel-lean and low fuel flow rate conditions. This level of CO emissions indicates that the SRB is acceptable for practical applications and the emission performance is even better than the conventional porous radiant burners for most operating conditions [17]. At very fuel-lean conditions, CO emissions rapidly increase with decreasing fuel flow rates. This tendency is observed since the flame temperature is very low and thus oxidation (to carbon dioxide, CO₂) rates are reduced. At moderate to high fuel flow rates (>1400 sccm) CO emissions do not seem to be sensitive to both the fuel flow rate and ϕ . Considering that CO emissions are expected to be sensitive to flame location since the oxidation time is reduced as the flame approaches the exit plane of the PM2 [17], this observation seems to be reasonable because flame does not move remarkably at those conditions, particularly for various fuel flow rates, as discussed in Section 3.2. If fuel flow rates increase further beyond the present test conditions, CO emissions are expected to increase due to the limited oxidation time. As briefly discussed in Section 3.2 (Fig. 6), further studies regarding the effects of the flame position on the SRB performance, including CO emissions, are needed when the overall performance of practical systems is considered.

The emissions of NO_x from the exhaust gas as a function of fuel flow rates for premixed C₃H₈/air flames of various fuel-equivalence ratios ($\phi = 0.3–0.6$) in the SRB at NTP are given in Fig. 10. All the NO_x concentrations in the figure are corrected to 15% O₂. For a

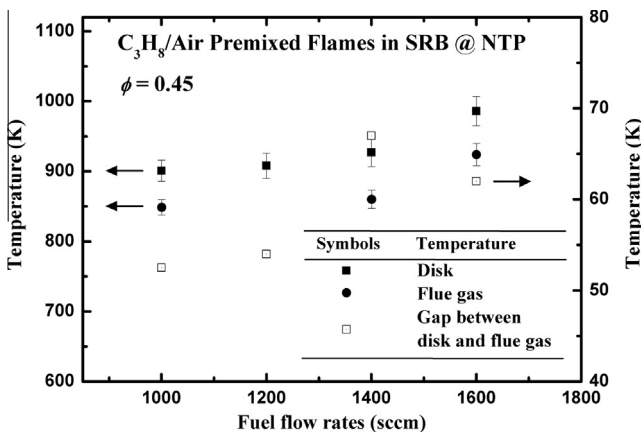


Fig. 8. Disk and flue gas temperature in terms of fuel flow rates for premixed C₃H₈/air flames of $\phi = 0.45$ in SRB at NTP.

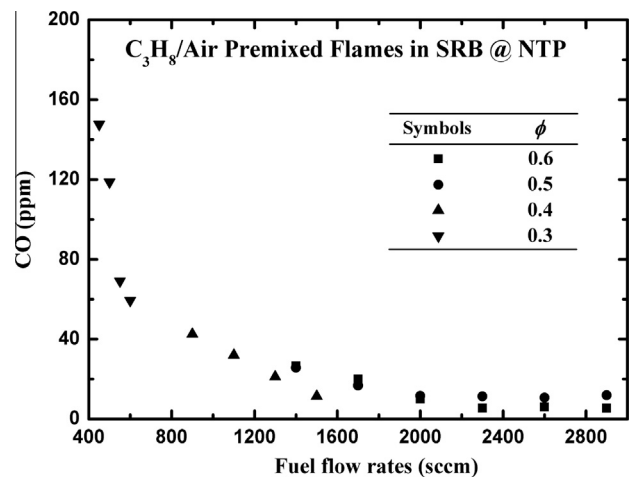


Fig. 9. CO emissions from exhaust gas as function of fuel flow rates for premixed C₃H₈/air flames of various fuel-equivalence ratios in the SRB at NTP.

given ϕ the NO_x concentration increases with increasing fuel flow rates in general, which is observed since the peak temperature that is enhanced due to the intensified burning (as shown in Figs. 6 and 7) strongly affects NO_x emissions via a thermal mechanism. For a fixed fuel flow rate, however, no consistent tendency in terms of ϕ is observed. Actually, some earlier studies on the NO_x emissions of porous radiant burners have shown conflicting results, i.e., different tendencies of emissions for varying ϕ and V [9,17]. Thus, the effects of ϕ and V on NO_x emissions are less clear. This unclear tendency seems to be observed since the peak temperature that strongly affects NO_x emissions via a thermal mechanism, particularly for fuel-lean condition, varies with varying ϕ and V , but simultaneously the residence time of burned gas also varies due to the flame position that is changed with ϕ and V , which may compensate the effects of the varied peak temperature. Also, the earlier study shows that NO_x emissions can be substantially reduced when the materials of porous medium are replaced, e.g., SiC [9]. Thus, further studies regarding the effects of the SRB materials as well as the flame position on the SRB performance (including NO_x emissions) are needed when the overall performance of practical systems is considered. Considering that the absolute NO_x concentration is between 2 and 7 ppm for all the present test conditions, however, finding a general tendency may not be meaningful since any variations are likely to be within the measurement error. This level of NO_x emissions, which is well below the general standards, e.g., 70 ppm for commercial burners by Southern California Emission Standards, indicates that the SRB is acceptable for practical applications and the emission performance is even better than the conventional porous radiant burners for most operating conditions [17].

As a final item of investigation, the thermal efficiencies of the present SRB are estimated and given in Fig. 11, which shows thermal efficiencies as a function of fuel flow rates for premixed $\text{C}_3\text{H}_8/\text{air}$ flames of various fuel-equivalence ratios ($\phi = 0.3\text{--}0.6$) in the SRB at NTP. In the present study, the thermal efficiency is defined as follows:

$$\eta = \frac{\dot{Q}_f - \dot{Q}_{\text{exh}}}{\dot{Q}_f} = 1 - \frac{\dot{m}_{\text{exh}} c_{p,\text{exh}} (T_{\text{exh}} - T_{\text{amb}})}{\dot{Q}_f} \quad (1)$$

where \dot{Q}_f , \dot{Q}_{exh} , \dot{m}_{exh} , $c_{p,\text{exh}}$, T_{exh} and T_{amb} are the input heat power of fuel (based on lower heating value), the exhausted heat rate, the mass flow rate of the exhaust gas, the specific heat of the exhaust gas at constant pressure, the exhaust gas temperature behind the

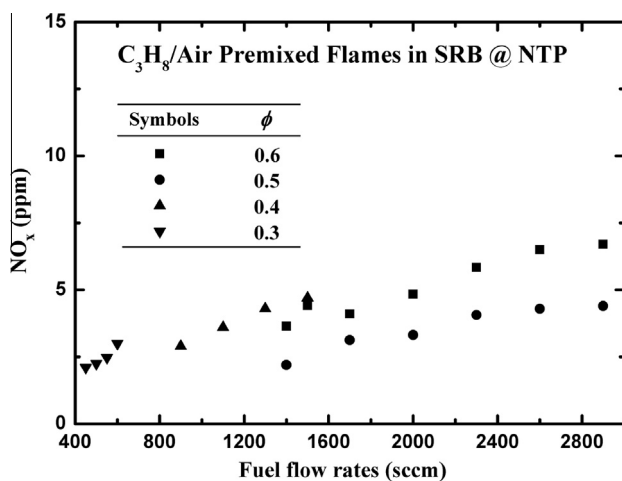


Fig. 10. NO_x emissions from exhaust gas as function of fuel flow rates for premixed $\text{C}_3\text{H}_8/\text{air}$ flames of various fuel-equivalence ratios in the SRB at NTP.

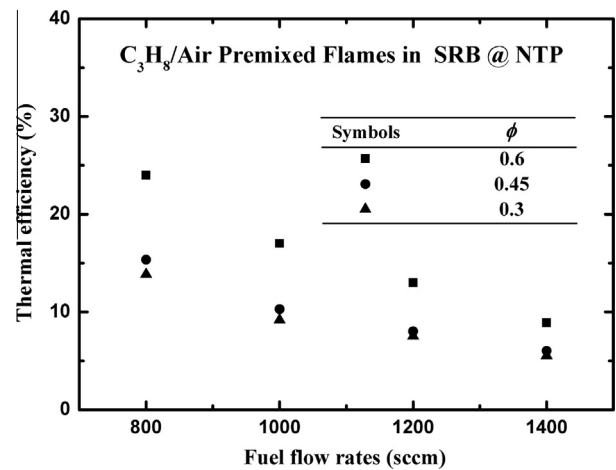


Fig. 11. Thermal efficiencies as function of fuel flow rates for premixed $\text{C}_3\text{H}_8/\text{air}$ flames of various fuel-equivalence ratios in the SRB at NTP.

preheater and the ambient temperature, respectively. As shown in the figure, η decreases with increasing fuel flow rates, due to enhanced heat losses even with the increased fuel input. Meanwhile, η increases with increasing ϕ , which is predicted from the earlier computational study showing a similar tendency up to $\phi \approx 0.5$ until the flame moves to the burner inlet and thus more radiation loss occurs [4]. According to Eq. (1), the thermal efficiencies of the SRB are expected to be enhanced compared with the conventional porous radiant burners since T_{exh} decreases due to the substantial heat recovery through the preheater. Actually, the earlier computational study of the SRB has shown η even higher than 40% under the optimized condition compared with at most 25% for conventional porous radiant burners [4]. Of course, such a substantial improvement in η can be attributed to the unique feature of the SRB, the external heat recirculation via the preheater and the efficient heat transfer through the radiation rods. For the configuration and materials of the present SRB under the present test conditions, however, η is lower than 25%, which is just a similar level to the conventional porous radiant burners. This significant difference between the earlier prediction and the present measurements in η of the SRB seems to be caused by the difference between the ideal computational condition and the actual experimental condition. For instance, it is expected that there are remarkable heat losses, though the side walls of the SRB are assumed to be perfectly insulated for the computations. Also, a small gap at the interface between the PM1 and PM2, which cannot be completely avoided in the experiments, plays a role as a flashback arrestor along with the small-pored upstream PM1. Since the interface is ideally considered without any physical gap for the computations, however, the flame can move into the porous medium just with smaller pores (PM1) through it, not resulting in the flashback extinction. Actually, most computed flames have been predicted to be stabilized in the PM1 [4], while the present measured flames are observed only in the PM2. Finally, the present SRB has not been optimally designed considering various parameters as aforementioned. Thus, in the present investigation neither the configuration and dimensions nor the test operating conditions have been optimized. Although the computational and experimental studies have been conducted using the SRBs with different configurations at different test conditions, a rough comparison of the results indicates the present values of η under non-optimized conditions seem to be reasonable. Thus, it is expected that significantly improved thermal efficiencies can be experimentally obtained if a new SRB is optimally designed with new materials, extending the

combustion stability limits by considering various design and operating parameters.

4. Conclusions

In the present investigation the potential of the concept of a radiant porous burner with augmented preheating (i.e., superadiabatic radiant burner, SRB) was experimentally evaluated, motivated by the earlier computational study of the SRB showing several unique features. A SRB was designed and fabricated, and the combustion stability limits and temperature distribution of premixed C_3H_8 /air flames in the SRB at NTP and the CO and NO_x emissions and efficiencies of the SRB were measured. The major conclusions of the study are as follows:

1. The porous alumina SRB with a square cross-section has been fabricated, which consists of a small-pored upstream section for internally preheating the incoming gas mixture, a large-pored downstream section for establishing flame, a preheater for externally recovering heat from the exiting flue gas and preheating the inlet air for the burner in addition to the internal heat recirculation in the small-pored upstream section, and radiation rods for extracting heat from the flame and transferring it to radiating disk surfaces.
2. The SRB can be operated even at very fuel-lean condition because of the external heat recirculation as well as the internal heat recirculation, showing blow-off and flash-back limits for a given fuel-equivalence ratio.
3. The superadiabatic effects have been experimentally demonstrated, showing that the superadiabatic radiation temperature on the disk surfaces is higher than the flue gas temperature at the same axial location, which confirms the previous theoretical and computational results of SRBs.
4. The emissions of CO and NO_x well below the general standards indicate that the SRB is acceptable for practical applications and the emission performance is even better than the conventional porous radiant burners for most operating conditions.
5. It is expected that significantly improved thermal efficiencies can be experimentally obtained if a new SRB is optimally designed with new materials, extending the combustion stability limits by considering various design and operating parameters.

Acknowledgment

This research was supported by Basic Science Research Program through the National Research Foundation of Korea (NRF) funded by the Ministry of Education (No. 2013R1A1A2006403).

References

- [1] Wood S, Harris AT. Porous burners for lean-burn applications. *Prog Energy Combust Sci* 2008;34:667–84.
- [2] Abdul Mujeeb M, Abdullah MZ, Abu Bakar MZ, Mohamad AA, Abdullah MK. Applications of porous media combustion technology – a review. *Appl Energy* 2009;86:1365–75.
- [3] Al-Hamamre Z, Diezinger S, Talukdar P, von Issendorff F, Trimis D. Combustion of low calorific value gases from landfills and waste pyrolysis using porous medium burner technology. *Process Saf Environ* 2006;84:297–308.
- [4] Vandadi V, Park C, Kaviany M. Superadiabatic radiant porous burner with preheater and radiation corridors. *Int J Heat Mass Trans* 2013;64:680–8.
- [5] Hsu P-F, Evans WD, Howell JR. Experimental and numerical study of premixed combustion within nonhomogeneous porous ceramics. *Combust Sci Technol* 1993;90:149–72.
- [6] Durst F, Trimis D. Combustion by free flames versus combustion reactors. *Clean Air* 2002;3:1–20.
- [7] Delalic N, Mulahasanovic D, Ganic EN. Porous media compact heat exchanger unit-experiment and analysis. *Exp Therm Fluid Sci* 2004;28:185–92.
- [8] Vogel BJ, Ellzey JL. Subadiabatic and superadiabatic performance of a two-section porous burner. *Combust Sci Technol* 2005;177:1323–38.
- [9] Gao HB, Qu ZG, Feng XB, Tao WQ. Methane/air premixed combustion in a two-layer porous burner with different foam materials. *Fuel* 2014;115:154–61.
- [10] Al-attab KA, Ho JC, Zainal JA. Experimental investigation of submerged flame in packed bed porous media burner fueled by low heating value producer gas. *Exp Therm Fluid Sci* 2014;62:1–8.
- [11] Keramiotis Ch, Katoufa M, Vourliotakis G, Hatzia Apostolou A, Founti MA. Experimental investigation of a radiant porous burner performance with simulated natural gas, biogas and synthesis gas fuel blends. *Fuel* 2015. <http://dx.doi.org/10.1016/j.fuel.2015.06.041>.
- [12] Kotani Y, Behbahani HF, Takeno T. An excess enthalpy flame combustor for extended flow ranges. *Proc Combust Inst* 1984;20:2025–33.
- [13] Qiu K, Hayden ACS. Thermophotovoltaic power generation systems using natural gas-fired radiant burners. *Sol Energy Mater Sol Cells* 2007;91:588–96.
- [14] Smucker MT, Ellzey JL. Computational and experimental study of a two-section porous burner. *Combust Sci Technol* 2004;176:1171–89.
- [15] Joo JM, Lee S, Kwon OC. Effects of ammonia substitution on combustion stability limits and NO_x emissions of premixed hydrogen-air flames. *Int J Hydrogen Energy* 2012;37:6933–41.
- [16] Gordon S, McBride BJ. Computer program for calculation of complex chemical equilibrium compositions and applications. Cleveland, OH, USA: NASA Report RP-1311-P2; 1996.
- [17] Khanna V, Goel R, Ellzey JL. Measurements of emissions and radiation for methane combustion within a porous medium burner. *Combust Sci Technol* 1994;99:133–42.